Real-Time Monitoring of Aluminum Crevice Corrosion and Its Inhibition by Vanadates with Multiple Beam Interferometry in a Surface Forces Apparatus

Buddha Ratna Shrestha,[a,*] Qingyun Hu,[a] Theodoros Baimpos,[a] Kai Kristiansen,[b] Jacob N. Israelachvili,[b,z] and Markus Valtiner[a,z]

[a]*Department of Interface Chemistry and Surface Engineering, Max-Planck Institut für Eisenforschung GmbH, D-40237 Düsseldorf, Germany*
[b]*Department of Chemical Engineering, University of California, Santa Barbara, California 93106, USA*

Crevice corrosion (CC) of metals remains a serious concern for structural materials. Yet a real-time in situ visualization of corrosion, and its inhibition within a confined geometry, remains challenging. Here, we present how multiple-beam interferometry in a Surface Forces Apparatus can be utilized to directly visualize corrosion processes in real-time and with Ångstrom resolution within well-defined confinement geometries. We use atomically smooth muscovite mica surfaces to form round-shaped ~1000 μm^2 crevices on aluminum. After exposure to NaCl solutions we can detect and track active sites of aluminum corrosion within this confined geometry. CC of aluminum randomly initiates in the confined crevice mouth, where the distance between apposing surfaces is between 20–300 nm. We can directly track oxide dissolution/formation, and corrosion-rates as well as their retardation due to sodium vanadate inhibitors present in solution. Formation of a compacted oxide layer effectively inhibits CC in 5 mM NaCl solutions with 2.5 mM of added $NaVO_3$, while inhibition rapidly breaks down at chloride concentrations above 50 mM. Breakdown of the inhibition-layers is initiated by rapid dissolution of the protective oxide within the confined zone. Our technique may be adapted for monitoring CC, corrosion inside of crack-tips, and evaluation of inhibitor efficiencies in a variety of metals.
 [DOI: 10.1149/2.0501507jes]

Manuscript submitted February 6, 2015; revised manuscript received March 30, 2015. Published April 9, 2015.

Aluminum is a light metal with only one-third of the density of steel, yet can be very tough as high-strength aluminum alloys have ultimate tensile strengths (UTS) approaching 690 MPa.[1] As such, aluminum and its alloys have become essential in diverse engineering applications and areas, such as structural materials design in the aviation, aerospace and marine industries, as well as in the food and beverage industries. Besides its light weight, one of the prime reasons for the wide use of aluminum is its good-to-excellent resistance to corrosion due to the formation of a passivating oxide layer when it is exposed to ambient atmospheres[2–5] and which can be further increased by an anodizing procedure. The naturally formed-oxide layer is only a few nanometers thick,[6] but is very stable, well adhering, and effectively protects the bulk aluminum metal from corrosion.

An openly exposed aluminum surface can resist quite severe corrosive environments such as mild acids.[1] Yet, passive films are susceptible to localized breakdown[7] and attack in confined situations,[8] especially in environments that contain corrosive anions such as chlorides.[3,4,9,10] Chlorides are, however, abundant in the environment, and in particular at shoreline locations close to seawater. An effective and durable protectant against corrosion in chloride-rich environments is therefore essential for the safe use of aluminum-based structural materials. Depending on the detailed exposure conditions under which localized break down of the passivation layer occurs, the corrosion of aluminum is classified as 'pitting corrosion' or 'crevice corrosion'. Pitting corrosion refers to situations where corrosive attack initiates and causes a localized break down on an extended surface that is openly exposed to the corrosive environment. Crevice corrosion refers to corrosive attack that occur when an aluminum surface is in close proximity to another 'apposing' surface, for example, an oxide or polymer film, a metal bolt in an engineered structure, etc.

Ex situ analyses of pitting corrosion,[9,11–14] crevice corrosion[5,12] and uniform corrosion of aluminum[15] in different media have been investigated in numerous experimental studies. However, a real-time and in situ investigation of localized corrosion (either pitting or crevice corrosion) remains a rather difficult task: Localized corrosion processes take place at very small scales and highly localized initiation sites[12] that may be buried or hidden within a confined geometry of two apposing surfaces. Similarly, a direct in situ view into processes at progressing crack tips is experimentally difficult. Typically, electrochemical pitting corrosion and crevice corrosion tests are carried out in a representative environment, and the sample surfaces are then examined ex-situ using a variety of different techniques.[16–18] Initial pit-formation can be studied in situ by scanning probe imaging techniques such as electrochemical scanning tunneling microscopy (EC-STM),[19] electrochemical atomic force microscopy (EC-AFM)[20] or scanning kelvin probe force microscopy (SKPFM).[21] But even EC-STM and EC-AFM or SKPFM do not always detect pitting corrosion since the initiation sites are sparsely distributed, and just after initiation the subsequent pit propagation cannot be visualized inside the active environment.

Even though, in principle, it is experimentally possible to monitor initial pitting corrosion at an openly exposed surface, a real time monitoring of crevice corrosion or the internal pit site is extremely challenging. Lead-in-pencil or artificial pit electrodes,[22–27] Normansky interference contrast microscopy,[5] artificial crevices techniques,[28] X-ray micro-tomography,[29] synchrotron based micro-tomography,[30] as well as electrode arrays[31] have all been used to study crevice corrosion under various conditions. However, to our knowledge, an Ångstrom resolved real-time visualization of the initiation of crevice corrosion inside a confined environment has not been experimentally demonstrated.

Here, we present Multiple Beam Interferometry (MBI (also known as White Light Interferometry, WLI) in a Surface Forces Apparatus (SFA) as a unique and powerful method for monitoring crevice corrosion in vapors or liquid solutions in the presence or absence of corrosion-inhibiting molecules. In this study, we use sodium vanadate, $NaVO_3$, as a model corrosion inhibitor of aluminum. Vanadates are potentially less carcinogenic candidates for the mandatory replacement of chromates as corrosion inhibition on aluminum in pigments and conversion coatings[32–34] that are used in the aviation industry. Using MBI in an SFA, we can track the formation of initial corrosive attack sites, the real-time dissolution (and therefore dissolution rate) of metal oxides inside an active crevice, and the area of the crevice corrosion attack. In addition, we can track in situ how effective inhibitor molecules are in different environments. Our setup may provide a

*Electrochemical Society Active Member.
[z]E-mail: jacob@engineering.ucsb.edu; valtiner@mpie.de

unique tool that can be extended to studying corrosion under confined situations, such as crack-tip propagation and/or crevice corrosion of other metals and alloys, provided that the surfaces or substrate films are reflective enough for performing white (in principle any type of light as UV and IR) light interferometry.

Materials and Methods

Chemicals.— All chemicals were purchased from Sigma-Aldrich at the highest purity available (sodium metavanadate = 99.9% pure). Solutions were prepared with Milli-Q (Millipore) water with a resistivity $\geq$18 MΩ cm^{-1} and a TOC $\leq$ 2 ppb. Optical grade 1 ruby-mica was obtained from S&J Trading Company (NJ, U. S. A.) as sheets of about 20 cm × 20 cm and 3 mm thickness. 5–10 cm^2 mica sheets with thicknesses ranging from 2–5 μm were hand-cleaved from raw sheets and used for the experiments. Edges of freshly cleaved thin mica sheets were melt-cut using a hot platinum wire in order to prevent clay swelling. Particular care was taken to avoid contamination of the mica sheets by Pt-particles. Physical vapor deposition (PVD) back-silvered mica sheets were cut and then glued to cylindrical silica disks of nominal radius of curvature $R = 7 – 15$ mm. Semitransparent Ag and Al thin films (45 nm) were prepared by PVD at deposition rates of $\leq$ 3 Å s^{-1}.

Surface forces apparatus (SFA).— SFA measurements were performed at 21°C in a cleanroom using the SFA 2000 model obtained from SurForce LLC (Santa Barbara, Cal., USA).[35] One cylindrical disc with an atomically smooth and back-silvered muscovite mica surface[36] and an apposing disc with a 45 nm thick aluminum layer were mounted in the SFA in a cross cylinder geometry. This creates a 2-layer interferometer[37] with the Al surface facing the solution side, while the back-silvered mica surface acts as the crevice former. Zero distance ($D = 0$) is defined as contact between mica and aluminum in dry argon gas. Any changes of the separation distance between the Ag and the Al "mirror" surfaces due to, e.g., ingress of water, or shift of the Al-mirror surface due to corrosion (conversion into oxide or dissolution), can be tracked in situ by following both the distance shift of the mirror *and* the change of the intensity (due to the thinning of the reflecting aluminum layer). The setup is sensitive to about 25–50 picometers absolute shifts of mirror distances, relative to the zero distance, $D = 0$, defined in dry argon gas. Further experimental details of WLI and MBI in an SFA are described in previous work.[38–40]

The Experimental Idea and Setup

Figure 1 shows a schematic of the experimental setup. In an SFA, a metal-coated (here aluminum-coated) glass cylinder and an apposing back-silvered mica sheet glued to another cylindrical glass surface, are mounted facing each other in a crossed-cylinder geometry (Fig. 1a), and brought together using a motor and piezo-driven approach mechanism into a well-defined flattened contact. One surface was mounted on a double-cantilever "force-measuring" spring (here with a spring constant of k~500 Nm^{-1}) through which the force between the two surfaces, F, can be controlled. A full schematic of the SFA setup is described in previous work.[38]

The initial contact was in a dry argon atmosphere (in the closed and atmospherically controlled SFA chamber). For establishing a flat contact, the atomically smooth and chemically inert mica surface acts as a "crevice former". The glue layer used to glue the back-silvered mica onto the cylindrical glass disc acts as compressible layer that, by adjusting the applied force, F, allows control of the confinement and flattened area, $A = \pi(\phi_i/2)^2$ with diameter ϕ_i of the area of contact, A. In the crossed-cylinder geometry the confined flattened region is circular. In this typical SFA setup, contact pressures can be precisely controlled and measured in situ.

Throughout an experiment, white light was guided through these apposing mirrors: the potentially corroding metal Al and Ag on the back side of the crevice forming mica that together form an interferometer. Constructive and destructive interference of discrete wavelength leads to the formation of so-called Fringes of Equal Chromatic Order (FECO) that are measured in a conventional grating spectrometer in real time – this being the basis of WLI or MBI.

For a detailed introduction of MBI the reader is referred to earlier work.[37] Briefly, a typical FECO image showing a flattened contact is shown in Figure 1b. The two dimensional FECO pattern or spectrum measured in the spectrometer simultaneously provides (i) the spectroscopic axis that gives the distance between the two apposing mirrors to better than 0.1 nm, and (ii) the lateral axis that provides an optical image of a section through the contact region with a (lateral) resolution of about ~0.7 μm.

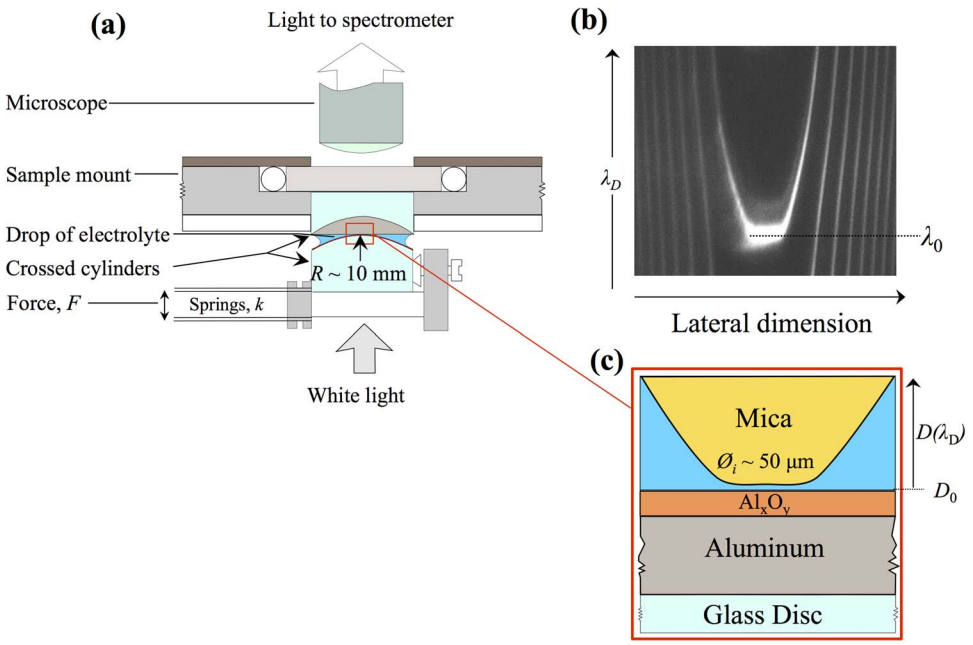

Figure 1. (a) Schematic of the experimental set up. (b) Shows a typical FECO that indicates a flat contact. (c) Schematic of the confined region (red rectangle) after a droplet of water is injected.

Using the microscopic lateral imaging capability of the SFA, the area of the formed flat and round shaped contact region (typical diameters are $\phi_i \sim 50$–100 μm) can be directly measured, and pressures, $P = F/A = F/\pi(\phi_i/2)^2$, can calculated based on the applied spring loading force, F. Here, we applied contact pressures of 3–4 atmospheres, and no direct influence of the applied pressure variation was found in this range. Also, in the initial contact situation in dry argon gas, the thickness of the mica can be directly measured from the FECO spectrum and the absolute zero distance, $D = 0$, is thereby defined.

As depicted in Figure 1c, in order to study crevice corrosion a drop of "potentially corrosive" electrolyte was injected between the two surfaces. Simultaneously, the defined crevice situation with a metal test surface (here aluminum) confined by a mica crevice former was continuously monitored in real time by recording the FECO at 2 frames per second (fps). This time resolution of 500 ms was sufficient for the present work, yet frame rates up to ~100 fps are possible with our current sensors. Continuous monitoring of FECO allowed in situ visualization and deciphering of the corrosive processes that occurred in confinement after exposure to corrosive environments by real time quantitative measurements of the following:

- The **intensity** of the transmitted light (fringes) through the two surfaces increases if the test surface (Al) starts to thin due to corrosive attack.
- The change in the **FECO fringe position** and hence the wavelength shift $\Delta\lambda$ away from λ_0 correlates with a shift ΔD of the metallic reflecting mirrors, that can be positive (expansion) or negative (contraction). This shift can be due to the surfaces coming closer together across the electrolyte solution (water gap), or dissolution of metal or metal oxide, or adsorption of additional material, salt or corrosion inhibitor. Also, formation of light absorbing layers, such as highly doped semiconductors or metallic layers with a high imaginary part of the refractive index can shift the wavelength, while simultaneously decreasing the transmitted intensity.
- The imaging capability of the SFA allows tracking of the 2D surface profile through a contact, and a 3D image can be obtained by laterally scanning or rotating the beam with a Dove prism. 3D recording has a lower time resolution, of minutes. Due to the fast corrosive breakdown we find in aluminum, in this work we focused only on fast 2D scanning of the corrosion site.

Results and Discussion

Here we describe how our setup works to monitor in real-time crevice corrosion of aluminum in the presence and absence of the corrosion inhibitor vanadate (e.g., $NaVO_3$) in 5 mM chloride (e.g., NaCl) solutions. We also investigated the corrosion inhibition efficiency of vanadate by increasing the concentration of chloride in the solution.

Monitoring a corrosion process under confined conditions in the presence and absence of $NaVO_3$.— After establishing and referencing $D = 0$ in dry contact between aluminum and a mica (crevice former) surface, a droplet of 5 mM NaCl solution with or without an additional 2.5 mM of $NaVO_3$ of pH ~ 5.5 was injected between the surfaces. The FECO spectrum was recorded, which, as previously described, results in both intensity changes and mirror shifts in the confined and wetted environment.

As shown in Fig. 2, in 5 mM NaCl solution (black data points) we found strong changes due to corrosion of the aluminum, while in solutions with an added 2.5 mM $NaVO_3$ (blue data points) we found little changes in the interfacial structure. Figure 2a compares the recorded change of intensity of transmitted light observed in 5 mM NaCl solution and in 5 mM NaCl with 2.5 mM $NaVO_3$. Here, the lowest intensity of transmitted light is defined as 0 and the maximum intensity is normalized to 1. These data were recorded in the center of the confined region. In 5 mM NaCl, we find that the intensity of the transmitted light (i.e., the FECO fringes) decreased slightly in the beginning, became scattered, then increased precipitously after about 3 hours to a maximum, accompanied by a broadening and

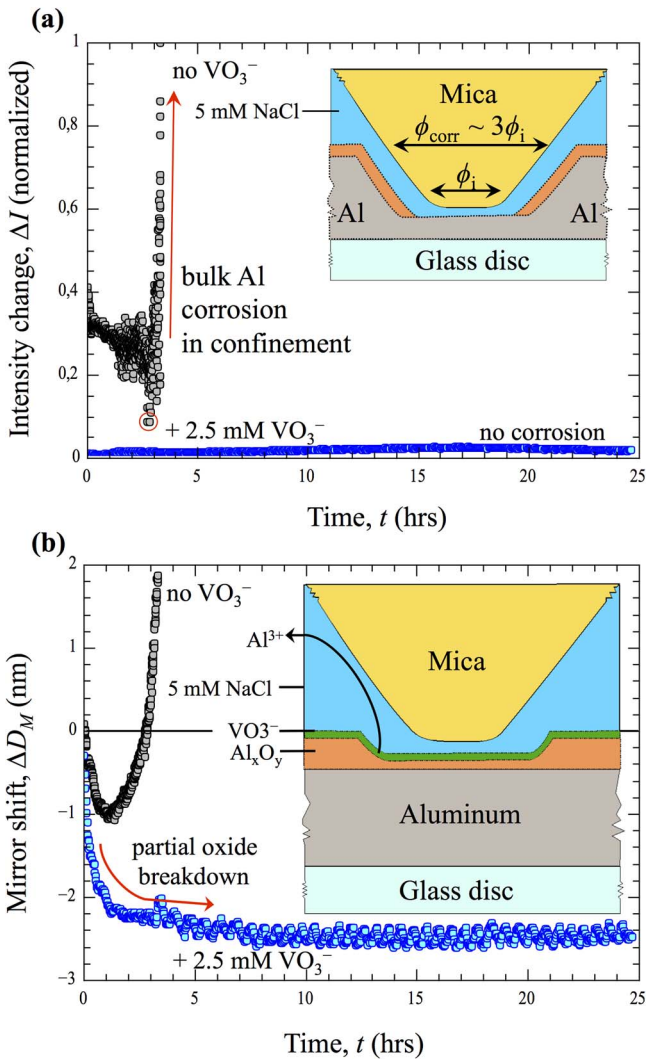

Figure 2. (a) Normalized intensity change as a function of time. At $t = 0$, 5 mM NaCl with and without 2.5 mM $NaVO_3$ was injected into the confined contact zone. The schematic indicates the corrosion of the entire confined region observed in 5 mM NaCl (*cf.* text for details). **(b)** Mirror shift as a function of time. The schematic indicates that the passive layer shrinks and alters upon ingress of vanadate ions.

eventual disappearance of the FECO fringes (see Fig. 3 later). This indicated that the aluminum layer fully corroded, i.e., was removed entirely. The initial decrease in the intensity of the transmitted light directly indicated that the ingressing electrolyte reacted with the metal (Al) giving rise to a light-absorbing corrosion product. It appeared that NaCl may have reacted[41] as well as incorporated[13,42–45] with/into the native oxide to form dissolved interfacial oxy-chloro compounds and/or a defect-rich and possibly semiconducting metal oxide phase. As such, both the initial decrease of light intensity, and the slight negative mirror shift (see Fig. 2b) have nothing to do with corrosion of the aluminum, but they indicate a chemical reaction and thinning of the passivating oxide layer. However, at this point in time we cannot provide a more detailed chemical view into the crevice and the intermediate species during this active process. Here, combination with in situ spectroscopic techniques may provide a more detailed insight in the future.

In addition, these results also show that it apparently takes about 3 hours to initiate an oxide breakdown. This suggests a correlation with the time needed to reach a critical concentration of interfacial chloride that is necessary to fully break down the passive oxide film,[17,18,46] (indicated by red circle in Fig. 2a). Once this critical concentration

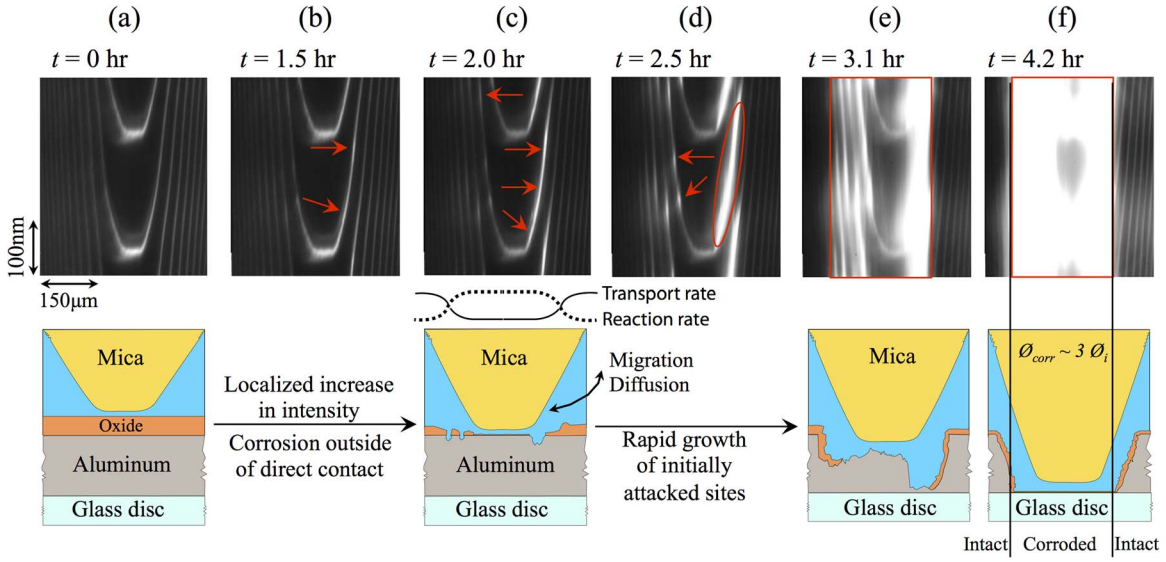

Figure 3. Consecutive 2D FECO images obtained as a function of time (indicated) after injection of 5 mM NaCl into a confined aluminum/mica contact. The schematics below show the progress of the corrosive reaction as deduced from the FECO images. As indicated in the schematic shown in Fig 3c a subtle balance between material transport rates (diffusion and migration) as well as reaction rates may control the locations where rapid CC initiation is most likely.

is reached, the passive layer breaks down quickly as suggested by our data, and consequently the exposed aluminum surface rapidly corrodes.

The results of Fig. 2 show that *only the confined aluminum becomes corroded* when it is exposed to 5 mM NaCl, as illustrated in the schematic in Fig. 2a. Experimentally, this can be directly seen in the FECO shown in Figure 3f, where the FECO outside the contact region are intact, with unaltered shape and intensity (discussed in detail below), while inside the contact all the initially reflecting aluminum layer has been removed.

Figure 2b shows the simultaneously recorded absolute mirror shifts during the corrosive attacks with 5 mM NaCl (black data points), and 5 mM NaCl with 2.5 mM $NaVO_3$ (blue data points and schematic inset). In 5 mM NaCl, we see that initially the mirrors gradually shift to shorter separations, indicating a thinning of the native oxide layer by ~1 nm. After about 3.5 hours, as the reaction progresses, the mirror distance shifts to larger separations at an increasingly faster rate. This reflects how the initial gradual dissolution of the native oxide film in the presence of chloride[47] transitions to corrosion of the now unprotected metal, where chloride and water both simultaneously react with the fully exposed aluminum surface leading to a rapid corrosive dissolution. The increase of the interfacial layer thickness may be due to corrosion product formation and/or swelling of the aqueous interfacial water layer due to rapid solvation of corrosion products.

In contrast, in the presence of $NaVO_3$, Fig. 2b shows a similar initial negative mirror shift distance of about 2 nm upon ingress of the electrolyte, suggesting that the native oxide is compacted as well. Together with the intensity change shown in Fig. 2a, this data supports the formation of a compacted vanadate/ oxide layer that is stable over the remaining 25 hours of exposure. In particular, Fig. 2a shows that the intensity increased slightly in the beginning, suggesting a chemically different interfacial process that is consistent with the formation of a passivating layer containing vanadate ions, followed by a constant (unchanging) transmitted intensity for the remaining 25 hours of the experiment. Formation of a stable and adherent VO_3^- containing layer and/or suppression of oxygen reduction by vanadate[48,49] could, therefore protect the passivating oxide layer on the surface.

The SFA-FECO method provides detailed information not only at one particular point within the confinement area: as already mentioned, the FECO spectrum represents a 2D 'image' through the corroding contact junction as well as outside of it. Figure 3 shows the full 2D FECO obtained at different times of the experiment described in Figure 2 performed in 5 mM NaCl, and a schematic illustration of the corrosion process at the interface. Initially (Fig. 3a), electrolyte is sandwiched between the aluminum oxide and mica surfaces. Figures 3b-3c show the FECO fringes at $t = 1.5$ and 2.0 hours, respectively, after wetting the confined region (at $t = 0$), which clearly shows that the transmitted intensity has increased in regions just outside the 'contact area', i.e., on the right and left curved arms of the FECO just outside the flat central (confined) region, while the intensity in the confined region has remained essentially unchanged. Similar region dependence on the dissolution phenomena has been reported for silica surfaces in close proximity to muscovite mica.[50] As already discussed above, an increase in the intensity at any particular location indicates that the aluminum in that location is dissolving away, allowing more light to pass through that point into the spectrometer. The FECO fringes also become much broader at these points due to a roughening of the metallic interface. By $t = 2.5$ and 3.1 hours (Fig. 3, 3d and 3e) new corrosion hot spots have appeared, grown, and spread even farther out from the center, indicating that the corrosion process involves lateral, depth, and areal expansion, i.e., strong roughening of the corroded surface.

This direct view into corrosion in confinement strongly suggests that corrosive attack starts in the opening of the crevice mouth *just outside* the intimate contact zone. In the system studied here, corrosive attack starts at locations where the two surfaces are separated by D = 20–300 nm. In general, this behavior is not uncommon for CC and was also observed e.g. for alloy 22.[51,52] It is however not immediately obvious, why CC should initiate and quickly progress just outside the intimate confinement zone. Therefore, one has to consider two competing processes, (i) the generally lower reaction rates further out of the intimate contact zone, as well as (ii) the competing material transport rates into and out of the crevice environment, which are slowest inside the intimate contact area. Consequently, a subtle balance between decreasing reaction rates and increasing rates of diffusion toward the outer confinement zone will naturally shift the most active region outside of the most intimate contact zone, at least during initiation of CC. Please also note, that the opening angle of our artificial crevices in both our schematic and the FECO are largely overestimated due to the lateral and vertical scale difference of ≥3 orders of magnitude (μm resolution in x/y and Å resolution in z). This large-scale confined region (over several 10's of μm the distance between the crevice former and Aluminum is just a few 100 nm) may also contribute to the very pronounced shift of CC out of the intimate

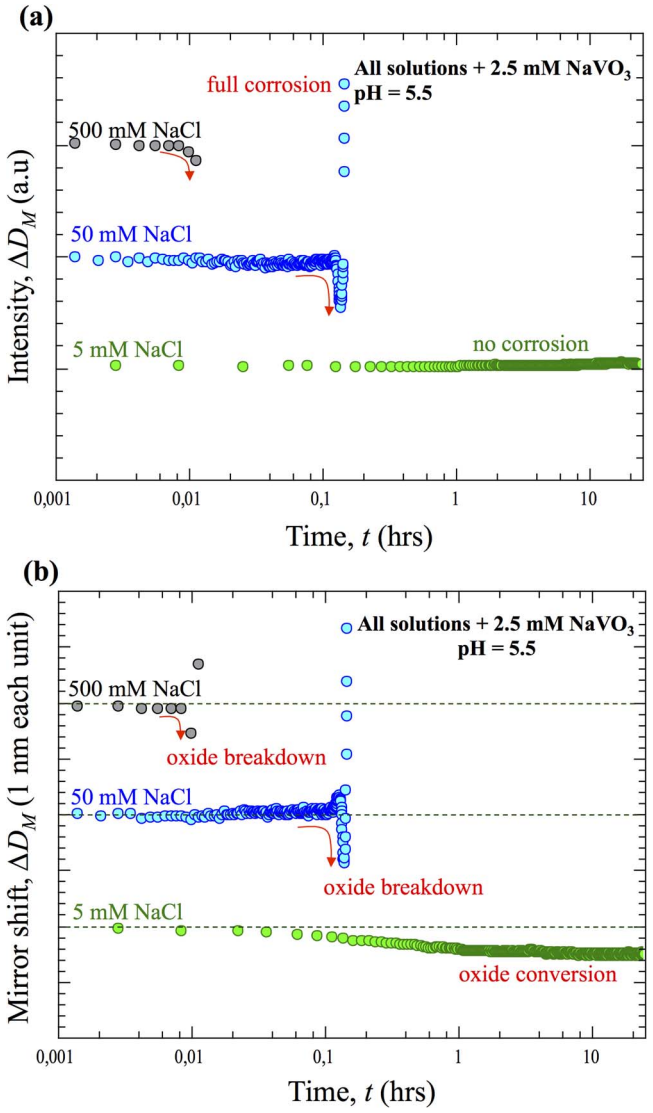

Figure 4. (a) Plot showing change in the (normalized) intensity of transmitted light with time in various solutions as indicated in the figure. (b) Plot showing mirror shift with time.

contact zone in these experiments. Related effects were observed in geological dissolution phenomena such as pressure solution,[50,53–55] and in a study where corrosion rates were monitored as a function of water film thickness.[56]

After 4.2 hours (Fig. 3f), the FECO just around the contact region, but now also within the confined region, have completely disappeared. Nevertheless, we still clearly see the FECO pattern well outside the confined region, beyond an area approximately 3 times the diameter of the initial flat contact, ϕ_i, where surfaces were $D \geq 300$–500 nm apart. This indicates that the metal corroded only within and immediately around the confined region, but not well outside it. The times indicated in Figure 3 also show that the corrosion process is (relatively) slow in the beginning and much more rapid later. Detailed chemical information may become accessible by combining FECO analysis with in situ spectroscopic techniques such as Raman or IR spectroscopy. This is however, beyond the scope of the current work.

Effect of chloride concentration on corrosion inhibition.— The effect of the chloride concentration on the inhibition efficiency of $NaVO_3$ was also tested, or more specifically, the 'critical' NaCl concentration above which 2.5 mM $NaVO_3$ no longer inhibits corrosion. Figure 4a shows the intensity change as a function of time for 5, 50 and 500 mM NaCl with 2.5 mM $NaVO_3$ as indicated in the figure. As already described, in case of 5 mM NaCl with 2.5 mM $NaVO_3$, corrosion was effectively inhibited for at least 25 hours. When the concentration of NaCl was increased to 50 mM, the oxide layer was quickly consumed and the confined metal dissolved away within ~350 s (6 min). In 500 mM solution it took only 40 s for the confined contact zone to be fully corroded.

Thus, aluminum corrosion in confinement zones is dramatically increased with an increasing NaCl concentration above some 'critical' value, and 2.5 mM of $NaVO_3$ is able to effectively inhibit corrosion only in quite low NaCl concentrations ($\leq$5 mM). We also tested how an increase of vanadate from 10 mM up to 50 mM in a 200 mM NaCl solution may inhibit or delay CC. Passivity breakdown in 10 mM $NaVO_3$ occurred after about 2.3 hours, while no passivity breakdown was observed in a solution with to 50 mM $NaVO_3$ over a monitored period of 4.5 hours. As such, these test cases shows how we can utilize this method to directly study in real time how effective given concentrations of corrosion inhibitors are in various corrosive environments over extended timescales.

More generally, the WLI in an SFA should be applicable to imaging and monitoring the corrosion of any metals and alloys in confined geometries. Even complex aspects such as effects of intermetallic particles may be accessible. The only prerequisite is that materials are reflective enough for performing white light interferometry, which is the case for most engineering metals and alloys. The technique may also be extended as a high-throughput method for in situ monitoring of crevice corrosion, stress corrosion cracking, and related phenomena. In particular, it may be used to rapidly evaluate the properties of corrosion inhibitors.

Finally, we want to emphasize that the interferometric technique used here was applied to deposited *thin film* materials, such as the 45 nm aluminum films, in *transmission* mode. WLI can also be applied in *reflection* mode to any bulk metals and alloys. Reflection mode is similarly accurate compared to transmission mode SFA and hence similar performance may be expected.[57]

Conclusions

- We utilized WLI in an SFA as a powerful tool for the real time monitoring of corrosion and corrosion inhibition in confined crevice geometries with millisecond resolution in time, Ångstrom resolution in distance separation and ~1 μm resolution in lateral distance.
- WLI provides the ability to directly visualize and monitor oxide dissolution/growth and metal dissolution in 2D and also 3D, under well-controlled externally applied pressures. It is also possible to obtain a detailed view into physical changes such as oxide dissolution. To a more limited degree also chemical changes occurring both around and within the confinement zone can be inferred. Here, combination of WLI and in situ spectroscopic tools (Raman or IR) may prove useful in the future.
- Using this newly developed method allowed establishing of 'critical' bulk concentrations of the corroding species (chloride) and/or corrosion inhibitor above or below which corrosion is effectively inhibited or initiated, respectively. For instance, in present work, 2.5 mM $NaVO_3$ effectively inhibited corrosion of aluminum in 5 mM NaCl solutions for 25 hrs. In solutions with 50 mM NaCl rapid break down of the native oxide occurred after about 3 h, resulting in rapidly progressing crevice corrosion.

Acknowledgments

B. R. S acknowledges the Max Planck Gesellschaft for Max Planck Fellowship; Q. H thanks cluster of Excellence (EXC 1069) Ruhr-University in Bochum and T. B. thanks the Alexander von Humboldt (AvH) foundation for financial support. K. K. and J. I. were supported by the Department of Energy, Office of Basic Energy Sciences, Division of Materials Sciences and Engineering, under Award DE-FG02-87ER-45331 (development of the SFA and white light optical

interference imaging technique, and first phase of corrosion measurements).

References

1. J. R. Davis, *Aluminum and Aluminum Alloys, Metals Handbook Desk Edition*, Asm International (1998).
2. T. P. Hoar and W. R. Jacob, *Nature*, **216**, 1299 (1967).
3. T. P. Hoar, *Corrosion Science*, **7**, 341 (1967).
4. J. Kruger, *International Materials Reviews*, **33**, 113 (1988).
5. J. O. Bockris and L. V. Minevski, *Journal Of Electroanalytical Chemistry*, **349**, 375 (1993).
6. I. Serebrennikova and H. S. White, *Electrochemical and Solid State Letters*, **4**, B4 (2001).
7. G. S. Frankel, *Journal Of Electrochemical Society*, **145**, 2186 (1998).
8. G. T. Moody, *Journal Of Chemical Society*, **89**, 723 (1906).
9. Z. Szklarsk., *Corrosion*, **27**, 223 (1971).
10. N. Sato, *Corrosion Science*, **31**, 1 (1990).
11. G. S. Frankel, R. C. Newman, C. V. Jahnes, and M. A. Russak, *Journal Of The Electrochemical Society*, **140**, 2192 (1993).
12. G. S. Frankel and N. Sridhar, *Materials Today*, **11**, 38 (2008).
13. P. M. Natishan and W. E. O'grady, *Journal Of The Electrochemical Society*, **161**, C421 (2014).
14. J. Soltis, *Corrosion Science*, **90**, 5 (2015).
15. K. D. Ralston, D. Fabijanic, and N. Birbilis, *Electrochimica Acta*, **56**, 1729 (2011).
16. J. A. Richardson and G. C. Wood, *Corrosion Science*, **10**, 313 (1970).
17. S. Hastuty, A. Nishikata, and T. Tsuru, *Corrosion Science*, **52**, 2035 (2010).
18. Y. Tsutsumi, A. Nishikata, and T. Tsuru, *Journal Of The Electrochemical Society*, **152**, B358 (2005).
19. V. Maurice, L. H. Klein, and P. Marcus, *Electrochemical and Solid State Letters*, **4**, B1 (2001).
20. P. Leblanc and G. S. Frankel, *Journal Of The Electrochemical Society*, **149**, B239 (2002).
21. V. Guillaumin, P. Schmutz, and G. S. Frankel, *Journal Of The Electrochemical Society*, **148**, B163 (2001).
22. H. H. Farrell, H. S. Isaacs, and M. Strongin, *Surface Science*, **38**, 31 (1973).
23. J. W. Tester and H. S. Isaacs, *Journal Of The Electrochemical Society*, **122**, 1438 (1975).
24. T. R. Beck, *Journal Of The Electrochemical Society*, **129**, 2412 (1982).
25. R. C. Newman and H. S. Isaacs, *Journal Of The Electrochemical Society*, **130**, 1621 (1983).
26. H. S. Isaacs, J. H. Cho, M. L. Rivers, and S. R. Sutton, *Journal Of The Electrochemical Society*, **142**, 1111 (1995).
27. Q. Meng, T. Ramgopal, and G. S. Frankel, *Electrochemical and Solid State Letters*, **5**, B1 (2002).
28. E. Akiyama and G. S. Frankel, *Journal Of The Electrochemical Society*, **146**, 4095 (1999).
29. B. J. Connolly, D. A. Horner, S. J. Fox, A. J. Davenport, C. Padovani, S. Zhou, A. Turnbull, M. Preuss, N. P. Stevens, T. J. Marrow, J. Y. Buffiere, E. Boller, A. Groso, and M. Stampanoni, *Materials Science and Technology*, **22**, 1076 (2006).
30. Y. Nakai, D. Shiozawa, and D. In, *Experimental Mechanics and Materials*, A. N. Binibrahim, M. Y. M. Sulaiman, W. S. W. Abdullah, M. R. Yusof, A. A. Abas, and K. M. Yazid Editors, P. 162 (2011).
31. T. Liu, Y. J. Tan, B. Z. M. Lin, and N. N. Aung, *Corrosion Science*, **48**, 67 (2006).
32. R. G. Buchheit, H. Guan, S. Mahajanam, and F. Wong, *Progress In Organic Coatings*, **47**, 174 (2003).
33. S. P. V. Mahajanam and R. G. Buchheit, *Corrosion*, **64**, 230 (2008).
34. I. J. Polmear and I. J. Arnold, London and Light Alloys Metallurgy Of The Light Metals, In *Metallurgy and Materials Science Series*, 3rd Ed., Butterworth-Heinemann (1995).
35. J. Israelachvili, Y. Min, M. Akbulut, A. Alig, G. Carver, W. Greene, K. Kristiansen, E. Meyer, N. Pesika, K. Rosenberg, and H. Zeng, *Reports On Progress In Physics*, **73**, 036601 (2010).
36. M. Valtiner, K. Kristiansen, G. W. Greene, and J. N. Israelachvili, *Advanced Materials*, **23**, 2294 (2011).
37. J. Israelachvili, *Journal Of Colloid and Interface Science*, **44**, 259 (1973).
38. T. Baimpos, B. R. Shrestha, S. Raman, and M. Valtiner, *Langmuir*, **30**, 4322 (2014).
39. S. Raman, T. Utzig, T. Baimpos, B. R. Shrestha, and M. Valtiner, *Nature Communications*, **5**, 5539 (2014).
40. B. R. Shrestha, T. Baimpos, S. Raman, and M. Valtiner, *Acs Nano*, **8**, 5979 (2014).
41. J. O. Bockris and Y. K. Kang, *Journal Of Solid State Electrochemistry*, **1**, 17 (1997).
42. A. Kolics, J. C. Polkinghorne, and A. Wieckowski, *Electrochimica Acta*, **43**, 2605 (1998).
43. P. M. Natishan, W. E. O'grady, E. Mccafferty, D. E. Ramaker, K. Pandya, and A. Russell, *Journal Of The Electrochemical Society*, **146**, 1737 (1999).
44. P. M. Natishan, S. Y. Yu, W. E. O'grady, and D. E. Ramaker, *Electrochimica Acta*, **47**, 3131 (2002).
45. S. Y. Yu, W. E. O'grady, D. E. Ramaker, and P. M. Natishan, *Journal Of The Electrochemical Society*, **147**, 2952 (2000).
46. Y. Tsutsumi, A. Nishikata, and T. Tsuru, *Corrosion Science*, **49**, 1394 (2007).
47. M. F. Abd Rabbo, G. C. Wood, J. A. Richardson, and C. K. Jackson, *Corrosion Science*, **14**, 645 (1974).
48. B. L. Hurley, K. D. Ralston, and R. G. Buchheit, *Journal Of The Electrochemical Society*, **161**, C471 (2014).
49. K. D. Ralston and R. G. Buchheit, *Ecs Electrochemistry Letters*, **2**, C35 (2013).
50. G. W. Greene, K. Kristiansen, M. Valtiner, J. Boles, and J. Israelachvili, *Geochimica Et Cosmochimica Acta*, **74**, A353 (2010).
51. A. K. Mishra and G. S. Frankel, *Corrosion*, **64**, 836 (2008).
52. K. J. Evans, A. Yilmaz, S. D. Day, L. L. Wong, J. C. Estill, and R. B. Rebak, *Jom*, **57**, 56 (2005).
53. N. Alcantar, J. Israelachvili, and J. Boles, *Geochimica Et Cosmochimica Acta*, **67**, 1289 (2003).
54. A. Anzalone, J. Boles, G. Greene, K. Young, J. Israelachvili, and N. Alcantar, *Chemical Geology*, **230**, 220 (2006).
55. E. E. Meyer, G. W. Greene, N. A. Alcantar, J. N. Israelachvili, and J. R. Boles, *Journal Of Geophysical Research-Solid Earth*, **111** (2006).
56. T. Tsuru, A. Nishikata, and J. Wang, *Materials Science and Engineering A-Structural Materials Properties Microstructure and Processing*, **198**, 161 (1995).
57. J. N. Connor and R. G. Horn, *Review Of Scientific Instruments*, **74**, 4601 (2003).